DOI: 10.1021/cg900654m

CRYSTAL GROWTH & DESIGN Article

2009, Vol. 9
5197–5205

# Precipitation of Iron and Aluminum Phosphates Directly from Aqueous Solution as a Function of Temperature from 50 to 200 °C

Teresa Roncal-Herrero,*,† Juan Diego Rodríguez-Blanco,‡ Liane G. Benning,‡ and Eric H. Oelkers†

†*Géochimie et Biogéochimie Experimentale, LMTG-Université de Toulouse-CNRS-IRD-OMP, 14 rue Edouard Belin, 31400 Toulouse, France, and* ‡*School of Earth and Environment, University of Leeds, LS29JT, United Kingdom*

*Received June 11, 2009; Revised Manuscript Received September 30, 2009*

**ABSTRACT:** The nucleation and crystallization of Al and Fe phosphate phases directly from aqueous solutions were investigated experimentally in batch reactors at 50 to 200 °C and pH 1.6. The mineralogy, elemental composition, and morphology of the formed solids were characterized by X-ray diffraction, spectroscopy, and high-resolution microscopic techniques. The corresponding dissolved aqueous Al, Fe, and P concentrations were analyzed by spectroscopic and chromatographic techniques. In all experiments Al and Fe phosphate phases readily precipitate from supersaturated solutions. Precipitation is initiated by the nucleation and growth of amorphous Al or Fe phosphate precursors. These crystallize at $T = 100$ °C to either variscite and metavariscite or strengite and phosphosiderite, respectively. At $T \geq 150$ °C, these Al and Fe amorphous phases recrystallize to either berlinite or ferric giniite, respectively. The composition of the aqueous solution in all cases evolves rapidly to near saturation with respect to variscite and strengite. These observations suggest that Al and Fe phosphates may be critical to limiting aqueous phosphate availability in many natural environments.

## 1. Introduction

Phosphate concentrations in natural waters have been of increasing concern to society. If these concentrations are too low, they may hinder forest and agricultural growth, but if they are too high, they may lead to eutrophication.[1,2] Thermodynamic calculations suggest that the Al and Fe phosphates variscite and strengite may control aqueous phosphate concentrations in acidic (pH < 7) environments.[3−6] This study is aimed at assessing experimentally the role of these minerals in controlling phosphate availability in natural waters by observing and quantifying the phases that precipitate directly from Fe, Al, and $PO_4$ bearing aqueous solutions as a function of temperature.

Variscite ($AlPO_4 \cdot 2H_2O$) and strengite ($FePO_4 \cdot 2H_2O$) are among the most common Fe and Al phosphates found in nature.[3] Structural arguments suggest that there is a complete solid solution between variscite and strengite.[7] Variscite, which has an orthorhombic crystal structure, is often found associated with metavariscite, which has the same chemical formula but is monoclinic. Both of these phases consist of a framework of alternating $PO_4$ tetrahedra and Al octahedra.[8,9] At high temperature, these phases dehydrate to form berlinite ($AlPO_4$). which consists of a framework of alternating $PO_4$ tetrahedra and Al tetrahedra.[10] Berlinite has similar industrial applications as quartz, due to its availability to resist corrosion and its similar piezoelectric properties; berlinite, however, has the advantage that it can be formed at lower temperatures.[11−13] Variscite and metavariscite are isostructural with strengite and phosphosiderite, respectively.[14,15] At temperatures greater than ~1000 K strengite and phosphosiderite dehydrate to form rodolocoite, a $FePO_4$ polymorph, which is isostructural with berlinite[16,17]

Variscite, metavariscite, strengite, and phosphosiderite have all been observed both in natural acid soils[4,18−27] and experiments.[28−37] Variscite and metavariscite form from the interaction of phosphate-rich meteoric waters with aluminum bearing rocks.[38] Berlinite occurs in combusted guano deposits.[39] Strengite and phosphosiderite usually appear associated; they both form as alteration products of phosphate pegmatite rocks at near surface conditions.[38] The iron phosphate phase ferric giniite $Fe_5(PO_4)_4(OH)_3 \cdot 2H_2O$ also forms as an alteration product of altered pegmatitic rocks.[15,19]

A number of previous studies provided insights into the behavior of aluminum phosphate precipitation in aqueous solutions and soils.[13,27,30,31,40,42] Variscite, metavariscite, and other hydrated aluminophosphates can be obtained from acid aqueous solution containing a P/Al molar ratio of 3.3[42] Cryptocrystalline aluminum phosphate precipitates from the interaction between double superphosphate fertilizers and acid soils.[27] Amorphous Al phosphate phases were observed to precipitate from aqueous solutions having a P/Al concentration ratio of 8 at ambient temperature; this precipitate transforms into pure variscite after 45 to 71 months at pH < 3.[31] 0.6 $\mu$m diameter crystalline variscite spheres were found to form at 98 °C from solution with a P/Al ratio of 1 at pH < 2 after 100 h of reaction.[30] Variscite and metavariscite can transform into berlinite at temperatures in excess of 150−200 °C.[13]

Other studies focused on characterizing iron phosphate precipitation in aqueous solutions.[17,37,43−45] Cryptocrystalline strengite and phosphosiderite have been reported to form from reaction between aqueous P and amorphous iron oxyhydroxide at 90 °C.[37] Strengite and phosphosiderite can be synthesized by either acid reflux or boiling[17,43] or at hydrothermal conditions.[44] The main industrial application of hydrated iron phosphates is their use as cathodes in Li batteries,[45−48] while giniite is used as a potential dehydrogenation catalytic material.[49]

*To whom correspondence should be addressed. E-mail: roncal@lmtg.obs-mip.fr. Telephone: +33(0)561 33 89 75. Fax: +33 0 561 33 25 60.



Published on Web 10/30/2009

Despite this past work, our understanding of the nucleation, growth, and transformation of Al and Fe phosphate minerals is still fragmented. Toward an improved understanding of these processes, the present study quantifies the temporal evolution of fluid and solid phases in supersaturated Al or Fe phosphate solutions under acid conditions as a function of temperature. The purpose of this paper is to report the results of this experimental study and to use these results to illuminate the role of iron and aluminum phosphates on aqueous phosphate availability in natural waters.

## 2. Materials and Methods

Five milliliters of aqueous 0.1 M $Fe(NO_3)_3 \cdot 9H_2O$ or $Al(NO_3)_3 \cdot 9H_2O$ solutions were mixed with 5 mL of an aqueous solution containing 0.1 M $KH_2PO_4$ and 0.09 M KOH in Teflon lined reactors. All solutions were prepared with 18 MΩ Milli-Q grade water, and the final pH for the $Fe^{3+}$, $Al^{3+}$, and $PO_4^{3-}$ stock solutions was 1.7, 1.6, and 4.8, respectively. pH was measured at 25 °C with an ORION pH-meter and a Toledo electrode calibrated with NBS standard buffer solutions. The low pH of the solutions avoided the formation of aluminum or iron hydroxides or mixed $OH^-$, $PO_4$ phases such as $Al(OH)_2H_2PO_4$.[50] Experiments were conducted at temperatures of 50, 100, 150, and 200 °C. All aqueous solutions were preheated prior to mixing. The solutions for the 50 °C experiments were preheated at 50 °C, while the solutions for the ≥100 °C experiments were preheated to 98 °C and then mixed in preheated reactors. The reactors were immediately sealed and placed in a preheated oven at the desired temperature.

The 100 °C experiments were run a maximum of 21 days and shaken three times per day. All other experiments were terminated after 12 h and shaken three times during this period. In all experiments, the 25 °C pH of the mixed fluids was ∼1.6. Fluid/precipitate suspensions were sampled regularly from the 100 °C experiments while in all other experiments the suspensions were sampled only at the end of runs. All samples were quenched to 25 °C immediately before sampling.

The quenched samples in all experiments were centrifuged at 13,000 rpm to separate solid and liquid phases. The liquid phase was filtered through a 0.2 μm polycarbonate filter. The final pH of the fluid phase at the end of each experiment was measured at 25 °C. Aqueous phosphate was measured by ion chromatography (IC) using a Dionex ICS 90. The filtered liquid phase was diluted with 0.1 M $HNO_3$ solution prior to further analysis. Aqueous aluminum concentrations were measured with an inductive coupled plasma optical emission spectrometer (ICP-OES) using a Perkin-Elmer Optima 5300DV, while total aqueous phosphorus and total aqueous iron were measured by absorbance spectrophotometry using a 3000Series UV/visible Cecil CE3041 spectrophotometer. Phosphorus was analyzed at a wavelength of 882 nm, using the ascorbic-molybdate blue method[51] while iron was analyzed at 562 nm following the ferrozine method.[52]

All solid phases were washed 3 times with Milli-Q water to remove excess salts and subsequently dried at room temperature. X-ray powder diffraction (XRD) analyses were performed using a Philips PW1050 diffractometer and Cu Kα radiation (λ = 1.5406 Å). Scans were recorded between 5 and 70° 2θ at a 0.1°/min scan rate and a step size of 0.08°. Patterns were compared to the standard mineral files compiled in the PDF2 database.[53] Midinfrared spectra of the solids were recorded from 650 to 4000 $cm^{-1}$ using an A2-Technology MicroLab Portable mid-IR spectrometer, with a diamond internal reflection (DATR) sampling system. Spectra were recorded with a 4 $cm^{-1}$ resolution by coadding 128 scans. Spectral manipulation including baseline adjustment, smoothing, normalization, and band component analysis was performed using the Thermo Nicolet OMNIC ESP 5.1 software package. Solids were imaged and analyzed using a LEO 1530 Gemini field emission gun scanning electron microscope (FEG-SEM), equipped with an Oxford Instrument energy dispersive X-ray (EDX) detector. Powders were placed on aluminum stubs, coated with a 3 nm platinum layer, and imaged at 3 keV and a working distance of 4 mm. Selected samples were also observed at high resolution using a Phillips/FEI CM200 FEG-transmission electron microscope (HR-FEG-TEM) equipped with an Oxford Instruments ISIS EDX system and selected area diffraction (SAED) capabilities. Samples were dispersed in ethanol and deposited on holey carbon TEM grids and imaged at 197 keV. The surface area of all solid samples was determined by the BET method,[54] using an 11-point nitrogen adsorption fit and a Micro-Quantachrome instrument with samples degassed at room temperature for 20 h prior to analyses.

## 3. Results and Discussion

The identity, size, morphology, and BET surface areas ($SA_{BET}$) of the formed solid phases for the aluminum and iron system are presented in Table 1. A summary of all experimental observations is provided in Figures 1 and 2. In all experiments an amorphous aluminum or iron phosphate phase with a spherical morphology precipitated immediately after mixing of the solutions. When analyzed after 12 h, the solids at 50 and 100 °C remained amorphous while, at higher temperatures, the amorphous phase recrystallized. Solids obtained from the 100 °C experiments after 9 or more days were also crystalline. In the Al-system variscite, metavariscite (both $AlPO_4 \cdot 2H_2O$) and berlinite ($AlPO_4$) formed while, in the Fe system, strengite, phosphosiderite (both $FePO_4 \cdot 2H_2O$), and ferric giniite ($Fe_5(PO_4)_4(OH)_3 \cdot 2H_2O$) formed. The surface area of the recovered solids generally decreases with increasing temperature. In the aluminum system, the specific surface area decreases from ∼82 $m^2/g$ for the solid synthesized at 50 °C for 12 h to ∼2 $m^2/g$ for the solid produced at 200 °C for 12 h. In the iron system, the specific surface area decreased from 152 $m^2/g$ for solid synthesized at 50 °C for 12 h to 10 $m^2/g$ for the solid produced at 150 °C for 12 h. XRD analyses confirmed the mineralogical composition, and the infrared spectroscopic analyses confirmed the continual

**Table 1. Identity, Size, Morphology, and Specific Surface Area of Solid Phases Recovered from the Aluminum and Iron Phosphate Experiments (AAP = Amorphous Al Phosphate; AFP = Amorphous Fe Phosphate)**

| nature of solid phase | *T* (°C) | experiment duration | identity of solid phase (XRD/SEM-EDX) | chemical formula | avg particle size (SEM/TEM) | particle morphology | $SA_{BET}$ ($m^2/g$) |
|---|---|---|---|---|---|---|---|
| amorphous | 50 | 12 h | AAP | $AlPO_4 \cdot xH_2O$ | – | spheres | 81.9 |
| | 50 | 12 h | AFP | $FePO_4 \cdot xH_2O$ | – | | 152.4 |
| | 100 | 12 h | AAP | $AlPO_4 \cdot xH_2O$ | 15 nm | spheres | – |
| | 100 | 12 h | AFP | $FePO_4 \cdot xH_2O$ | 20 nm | spheres | 66.7 |
| crystalline | 100 | 9 days | strengite | $FePO_4 \cdot 2H_2O$ | 1 μm | stars | 28.7 |
| | | | phosphosiderite | | 100 nm | prisms | |
| | 100 | 21 days | variscite | $AlPO_4 \cdot 2H_2O$ | 5 μm | bipyramid | 49.5 |
| | | | metavariscite | | > 100 μm | prisms | – |
| | 150 | 12 h | $AlPO_4 \cdot xH_2O$ | $AlPO_4 \cdot xH_2O$; $x = 1.1-1.3$ | 0.8 μm | tabular plates | 5.3 |
| | | | berlinite | $AlPO_4$ | 1 μm | hexagonal plates | – |
| | 150 | 12 h | ferric giniite | $Fe_5(PO_4)_4(OH)_3 \cdot 2(H_2O)$ | 5 μm | ball | 10.0 |
| | 200 | | ferric giniite | $Fe_5(PO_4)_4(OH)_3 \cdot 2(H_2O)$ | 2 μm | bipyramidal | – |
| | | | berlinite | $AlPO_4$ | 10 μm | hexagonal plates | 2.3 |

dehydration of the Al and Fe phases with increasing temperature and time.

The pH, aqueous composition, and saturation index of all fluid phases recovered at the end of each experiment with respect to selected Al and Fe phases are listed in Tables 2 and 3. The saturation indexes in these tables were calculated using PHREEQC[55] together with its llnl[56] database. The saturation indexes (S.I.) given in this table are defined by

$$\text{S.I.} = \log(\text{IAP}/K)$$

where IAP refers to the reaction activity quotient and $K$ designates the equilibrium constant of the phase of interest. The saturation index is thus positive when the solution is supersaturated with respect to the phase but negative when undersaturated. In both systems, amorphous phase

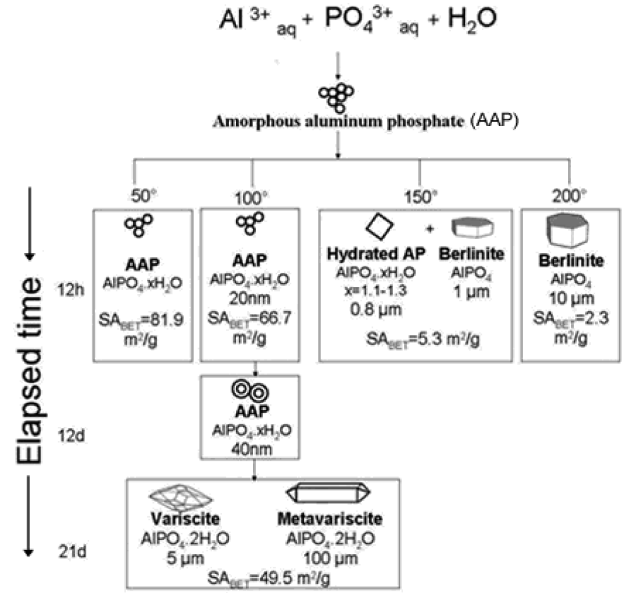


**Figure 1.** Summary of results obtained in the aluminum phosphate system as a function of time and temperature. The shape of the synthesized solid is indicated by the schematic illustration in each box.

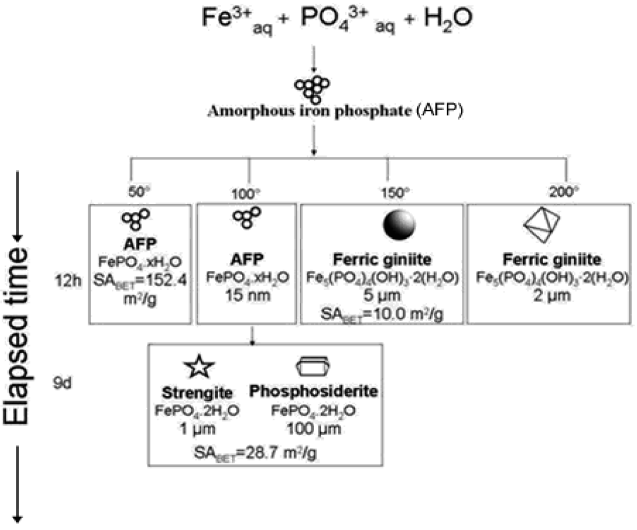


**Figure 2.** Summary of results obtained in the iron phosphate system as a function of time and temperature. The shape of the synthesized solid is indicated by the schematic illustration in each box.

precipitation (amorphous aluminum phosphate, AAP, and amorphous iron phosphate, AFP, respectively) occurs once the two aqueous solutions are mixed. 90% of the initial phosphate and aluminum or iron in aqueous solution was removed within the first minute, consistent with the precipitation of metastable amorphous phosphate phases via the Ostwald step rule.[57] These solids can recrystallize with time to form more thermodynamically stable phases. The transformation of pseudospherical AAP or AFP to crystalline phases is relatively slow at 100 °C; AAP persisted for at least 12 days, and AFP persisted for at least 9 days. This transformation rate is relatively slow compared to that of amorphous calcium phosphate (ACP), which transforms into crystalline brushite ($CaHPO_4 \cdot 2H_2O$) in less than 1 day at 25 °C.[58] In addition, amorphous calcium carbonate (ACC) transforms to crystalline $CaCO_3$ within 3 days at ambient temperature in a dry state[59] while in aqueous solution ACC transforms to crystalline $CaCO_3$ after ~5 min.[60]

Thermodynamic calculations performed using PHREEQC[55] suggest that, below 54 °C, the most stable phase in the Al phosphate system is variscite, while, at higher temperatures, berlinite is the stable polymorph. Corresponding calculations in the Fe phosphate system suggest that strengite is the most stable phase at all temperatures ≤200 °C, but these calculations were performed in the absence of thermodynamic properties for ferric giniite, which are not available in the literature. Thermodynamic calculations including metavariscite and phosphosiderite were also not possible due to the lack of data.

**3.1. Aluminum Phosphate System.** X-ray powder diffraction patterns and SEM images of solids obtained from the aluminum phosphate experiments are shown in Figures 3 and 4. The solids obtained after 12 h at 50 and 100 °C were amorphous aluminum phosphate (AAP), which at 100 °C transformed after 21 days into a mixture of variscite and metavariscite. Imaging revealed an isolated tabular prism of metavariscite of >100 $\mu$m length, embedded in a matrix of bipyramidal ~5 $\mu$m variscite crystals (see Figure 4a). Samples collected after 12 h of reaction at 150 °C consisted of a mixture of three-dimensional hexagonal berlinite crystals and hydrated aluminum phosphate which formed tabular platy crystals both ~1 $\mu$m in size (see Figure 4b). Samples collected after 12 h of reaction at 200 °C consisted of pure berlinite, again characterized by a hexagonal crystal habit, but at this temperature, the crystals were ~5−10 $\mu$m in size (see Figure 4b).

Further insight into the solid phase transformation process was obtained from the HR-TEM images of the solids collected from the 100 °C experiment at various times (Figure 5). The initial solids exhibit pseudospherical morphologies and diameters of 20 nm (Figure 5a). After 12 days of reaction at 100 °C (Figure 5b), the spheres grow, attaining a diameter of ~40 nm. An internal nucleus is apparent in some of these particles, although the structure remains amorphous, as indicated by the electron diffraction shown in Figure 5d. As mentioned above, the X-ray diffraction pattern in Figure 3 shows that this solid transforms into crystalline variscite and metavariscite after 21 days of reaction (see Figures 3b and 4a).

FTIR spectra of the various synthesized aluminum phosphate phases and the assignments for each spectrum are shown in Figure 6 and Table 4, respectively.[61−64] The most obvious changes upon heating are a decrease in the intensities and sharpening of the broad band between ~3000 and

**Table 2. Summary of the Fluid Chemistry in the Aluminum Phosphate Experiments, Showing Temperatures, Elapsed Times, Final pH, Concentration of Aqueous Species, as Well as log(IAP) and the Initial and Final Saturation Indexes (S.I.) for the Various Al Phases Present in the Experiments and Boehmite, $Al(OH)_3$, Calculated by PHREEQC**

| | | | | | log(IAP) | | S.I. | | | | | |
|---|---|---|---|---|---|---|---|---|---|---|---|---|
| | | | | | variscite, metavariscite, berlinite | | berlinite | | variscite | | boehmite | |
| *T* (°C) | experiment duration | pH | Al (mmol/L) | $PO_4$ (mmol/L) | initial | final | initial | final | initial | final | initial | final |
| 50 | 12 h | 1.7 | 39.16 | 35.74 | −19.90 | −20.10 | 0.91 | 0.72 | 1.1 | 0.9 | −2.65 | −2.71 |
| | 12 h | 1.7 | 36.53 | 23.76 | −19.87 | −21.02 | 3.3 | 2.16 | 1.13 | −0.01 | 0.01 | −0.92 |
| 100 | 21 days | 1.9 | 6.19 | | −19.87 | | 3.3 | | 1.13 | | 0.01 | |
| 150 | 12 h | 1.5 | 6.27 | 1.29 | −21.95 | −24.19 | 3.63 | 1.41 | −0.96 | −3.18 | 0.37 | −0.27 |
| 200 | 12 h | 1.4 | 6.15 | 1.33 | −23.60 | −25.81 | 4.56 | 2.36 | −2.6 | −4.8 | 1.4 | 0.74 |

**Table 3. Summary of the Fluid Chemistry in the Iron Phosphate Experiments, Showing Temperatures, Elapsed Times, Final pH, Concentration of Aqueous Species, as Well as the log(IAP) and the Initial and Final Saturation Indexes (S.I.) for the Various Fe Phases Present in the Experiments and Goethite, FeOOH, Calculated by PHREEQC**

| | | | | | log(IAP) | | | | S.I. | | | |
|---|---|---|---|---|---|---|---|---|---|---|---|---|
| | | | | | strengite, phosphosiderite | | ferric giniite | | strengite | | goethite | |
| *T* (°C) | experiment duration | pH | Fe (mmol/L) | $PO_4$ (mmol/L) | initial | final | initial | final | initial | final | initial | final |
| 50 | 12 h | 1.64 | | | −21.91 | | −125.12 | | 4.09 | | 2.68 | |
| | 12 h | 1.64 | 0.775 | 1.08 | −21.72 | −23.73 | −120.98 | −130.15 | 4.27 | 2.27 | 4.25 | 3.10 |
| 100 | 9 days | 1.48 | 0.027 | 0.23 | −21.72 | −25.67 | −120.98 | −140.49 | 4.27 | 0.33 | 4.25 | 0.53 |
| 150 | 12 h | 1.51 | 0.04 | 3.18 | −22.58 | −25.80 | −123.48 | −138.76 | 3.42 | 0.20 | 4.27 | 1.89 |
| 200 | 12 h | 1.4 | 0.01 | 3.24 | −23.62 | −27.73 | −126.98 | −146.40 | 2.37 | −1.73 | 4.77 | 1.76 |

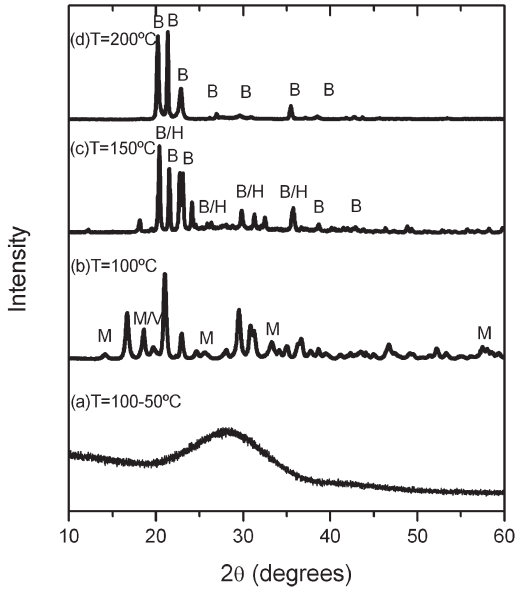


**Figure 3.** XRD patterns of solids obtained as a function of temperature during aluminum phosphate synthesis: (a) amorphous Al phosphate synthesized at 50 or 100 °C for 12 h; (b) metavariscite (M) and variscite (V); the 19.49 Å reflection is common for both minerals (M/V) synthesized at 100 °C for 21 days; (c) $AlPO_4 \cdot xH_2O$; $x$ = 1.1−1.3 (H) and berlinite (B) synthesized at 150 °C for 12 h; (d) berlinite at 200 °C for 12 h. The latter patterns match closely the reference patterns for variscite (PDF 08-0157), metavariscite (PDF 33-0032), $AlPO_4 \cdot xH_2O$, $x$ = 1.1−1.3 (PDF 15-0265), and berlinite (PDF 20-0045).

3500 $cm^{-1}$ and a decrease in intensity of the band around ~1650 $cm^{-1}$. These bands represent water molecules associated with hydrated aluminum phosphate, O−H stretching, and H−O−H bending modes, respectively. The band at ~826 $cm^{-1}$ is assigned to the librational water mode. With increasing temperature, these bands sharpen or disappear due to water loss. This is in agreement with the XRD data that also showed that the water content of the solids decreases with increasing temperature; the solid is the dehydrated phase at 200 °C. The main phosphate bands are present between ~920 and ~1250 $cm^{-1}$. They either increase in intensity, as is the case for band no. 6, corresponding to a $PO_4$ stretching mode, or become sharper, as is the case for band no. 7, corresponding to a $PO_4$ symmetric stretching mode with increasing temperature. This reflects an increase in crystallinity and a change in $PO_4$ bonding within the structure of the formed phases. The bands at ~1050 $cm^{-1}$ (band no. 7) and ~946 $cm^{-1}$ (band no. 8) were assigned to P−O symmetric stretching modes of $PO_4$ units in the solids. Interestingly, the band at 947 $cm^{-1}$ should be IR inactive but is present due to the reduction of symmetry induced through the hydrogen bonding of water−phosphate.[63] $PO_4$ antisymmetric stretching vibrations appear at >1077 $cm^{-1}$. The presence of symmetric and antisymmetric vibrations suggest multiple $PO_4$ species in the solid sample.[63] Finally, the band at ~700 $cm^{-1}$ (band no. 10) corresponds to the Al−O mode,[61−64] and it increases in intensity with increasing temperature (see Figure 6). Spectrum d in Figure 6 represents pure berlinite formed after 12 h at 200 °C; the existence of this anhydrous phase is again confirmed by the absence of the water peaks in this spectrum.

**3.2. Iron Phosphate System.** X-ray powder diffraction patterns of synthesized iron phosphate phases (Figure 7) indicate that the solid formed after 12 h of reaction at 50 and 100 °C was amorphous iron phosphate (AFP). At 100 °C, this AFP transformed within 5 days into strengite and phosphosiderite dimorphs. After 12 h of reaction at 150 and 200 °C, ferric giniite with the chemical formula $Fe_5(PO_4)_4(OH)_3 \cdot 2H_2O$ was observed.

SEM photomicrographs of selected synthesized iron phosphates are shown in Figure 8 while HR-TEM images from the iron phosphate precipitates obtained at 50 °C after 12 h of reaction are presented in Figure 9. The HR-TEM images confirm that the AFP obtained at 50 °C was amorphous and

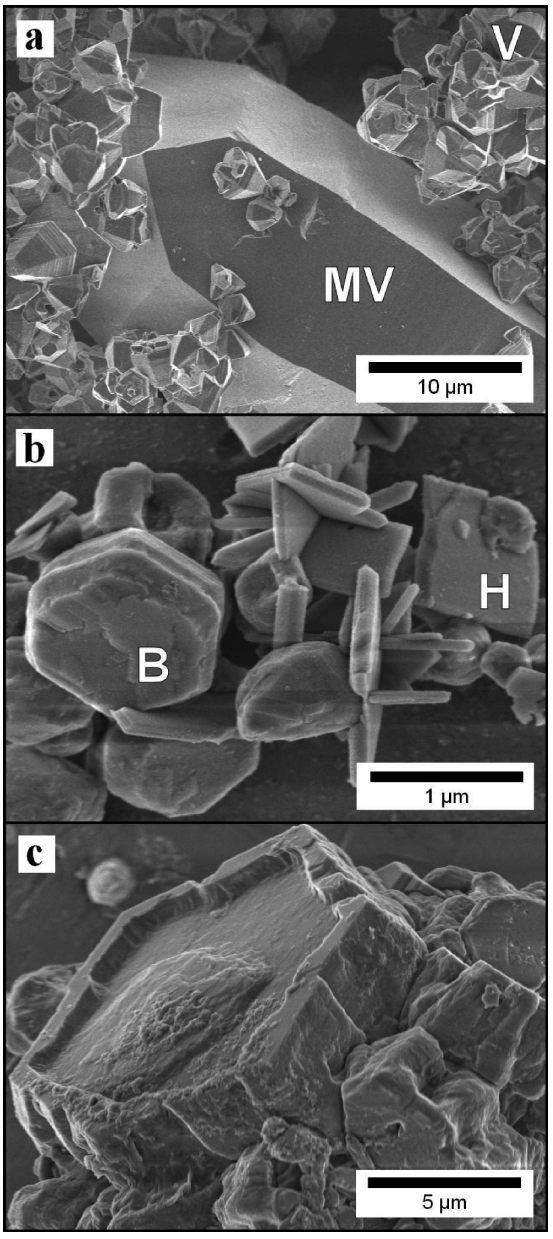


**Figure 4.** SEM photomicrographs of (a) variscite (V) and metavariscite (MV), synthesized at $T = 100$ °C for 21 days; (b) hydrous $AlPO_4 \cdot xH_2O$ (H) and berlinite $AlPO_4$ (B) synthesized at 150 °C for 12 h; (c) berlinite synthesized at $T = 200$ °C for 12 h.

consisted of grains that were ~20 nm in size. The solids recovered from the 100 °C experiments after 9 days of reaction consist of a mixture of 1 $\mu$m sized strengite stars and 100 nm phosphosiderite prisms (Figure 8a). At higher temperatures, ferric giniite is formed. Precipitated ferric giniite morphologies and sizes vary significantly with synthesis temperature. The 150 °C solids form rough 5 $\mu$m spheres (Figure 8b), and the 200 °C solids form 2 $\mu$m bipyramidal crystals with smooth surfaces (Figure 8c). Although these precipitated ferric giniite samples have different morphologies, their structure is identical, as demonstrated by the X-ray diffraction patterns (Figure 7c). Frost et al.[65] also produced synthetic ferric giniite from aqueous solutions at 120 °C after 2 days; their solids exhibited similar morphologies to those of the spherical crystals obtained in this study at 150 °C.

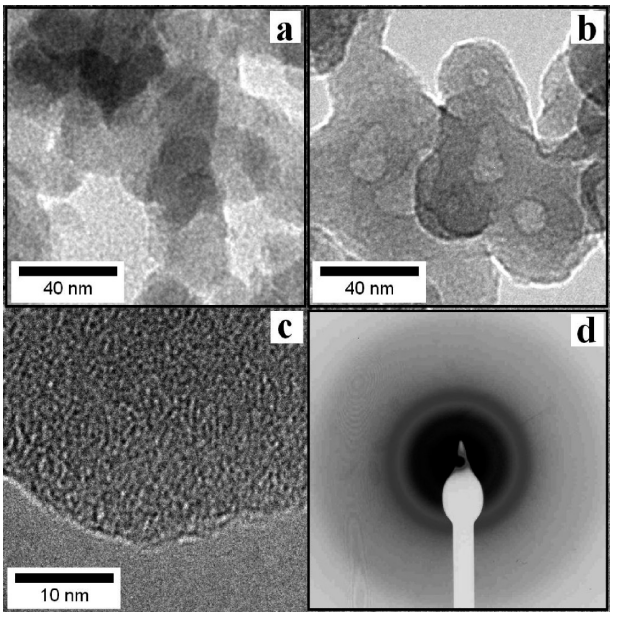


**Figure 5.** HR-TEM images of AAP obtained (a) just after mixing and (b) after heating at 100 °C for 12 days. (c) Details of a single AAP grain shown in part b. (d) Electron diffraction pattern of the grain shown in part c.

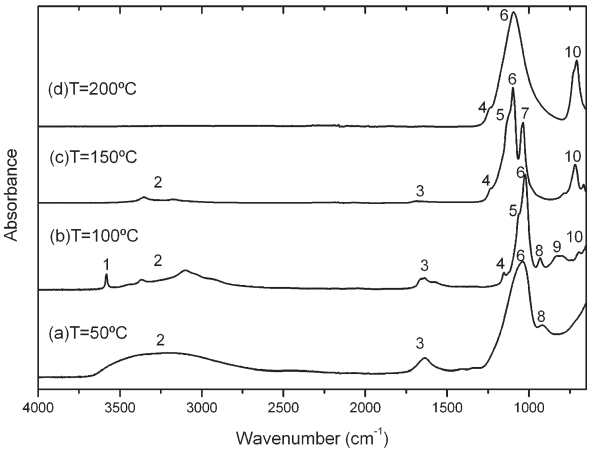


**Figure 6.** FTIR spectra of aluminum phosphates. Main bands are indicated by numbers above the spectra, and corresponding details of band assignements are described in Table 4 and in the text. (a) AAP synthesized at 50 °C taken from solution just after mixing; (b) variscite and metavariscite synthesized at 100 °C for 21 days; (c) hydrous $AlPO_4 \cdot xH_2O$ and berlinite synthesized at 150 °C for 12 h; (d) berlinite at 200 °C for 12 h.

FTIR spectra of the various synthesized iron phosphate phases and the assignments for each spectrum are shown in Figure 10 and Table 5, respectively.[62,63,65] The most obvious changes upon heating are a decrease in the intensities of bands no. 1 (not show in Figure 10) positioned between ~3000 and 3500 $cm^{-1}$ and a decrease in intensity of the band no. 3, around ~1650 $cm^{-1}$. These bands represent water molecules, O−H stretching, and H−O−H bending modes, respectively. With increasing temperature, these bands disappear due to water loss. The main phosphate bands are present between ~923 and ~1152 $cm^{-1}$. They either increase in intensity, as is the case for band no. 7, corresponding to a $PO_4$ stretching mode, or become sharper as with band no. 8, corresponding to a $PO_4$ symmetric stretching mode with

**Table 4. Main FTIR Bands for the Aluminum Phosphate Spectra in Figure 4**

| | wavenumber[a] ($cm^{-1}$) | | | | | |
|---|---|---|---|---|---|---|
| band no. | (a) | (b) | (c) | (d) | bonds assignments[b] | ref |
| 1 | | ~3595 | | | O−H $\nu$ | 63 |
| 2 | ~2659−3674 | ~2677−3543 | ~3000−3400 | | O−H $\nu$ | 63 |
| 3 | ~1648 | ~1647 | ~1650 | | H−O−H $\delta$ | 63 |
| 4 | | ~1168 | ~1250 | ~1256 | $PO_4$ $\nu$ | 63 |
| 5 | | ~1077 | ~1142 | | $PO_4$ $\nu$ | 62−64 |
| 6 | ~1051 | ~1038 | ~1112 | ~1110 | $PO_4$ $\nu$ | 62, 63 |
| 7 | | | ~1050 | | $PO_4$ $\nu$ | 62−64 |
| 8 | ~931 | ~946 | | | $PO_4$ $\nu$ | 63 |
| 9 | | ~826 | | | librational water | 63 |
| 10 | | ~708 | ~732 | ~723 | Al−O | 62−64 |

[a] (a) amorphous Al phosphate synthesized at 50 °C or 100 °C for 12 h; (b) metavariscite and variscite synthesized at 100 °C for 21 days; (c) $AlPO_4 \cdot xH_2O$, $x$ = 1.1−1.3, and berlinite synthesized at 150°C for 12 h; (d) berlinite synthesized at 200 °C for 12 h. [b] $\nu$ = stretching; $\delta$ = bending.

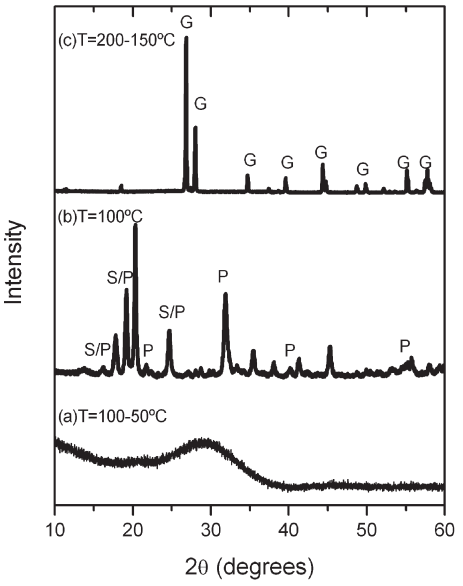


**Figure 7.** XRD patterns of iron phosphate solids obtained as a function of temperature during their synthesis: (a) amorphous Fe phosphate (AFP) synthesized at 50 or 100 °C for 12 h; (b) strengite (S) and phosphosiderite (P) synthesized at 100 °C for 9 days; (c) ferric giniite (G) at 150 or 200 °C after 12 h. The latter patterns match closely the reference patterns for strengite (PDF 15-0513), phosphosiderite (PDF 33-0666), and ferric giniite (PDF 45-1436).

increasing temperature. This reflects an increase in crystallinity and a change in $PO_4$ bonding within the structure of the formed phases. At higher temperature, phosphate peaks move to higher wavelengths, indicating that the structure becomes more ordered. $PO_4$ antisymmetric stretching vibrations appear at $> 1013\ cm^{-1}$. The presence of symmetric and antisymmetric vibrations suggests the presence of multiple $PO_4$ species in the solid sample.[60] For example, ferric giniite obtained after 12 h of reaction at 150 or 200 °C (Figure 10c) exhibits an antisymmetric stretching phosphate vibration at $1063\ cm^{-1}$ and symmetric stretching phosphate group vibrations at 989 and 923 $cm^{-1}$. The band at 923 $cm^{-1}$ may be ascribed to a second $PO_4^{3-}$ unit. This suggests that the phosphate units are not equivalent in the giniite structure.[65] Finally, the band at ~760 $cm^{-1}$ corresponds to the Fe−O mode,[62] and it increases in intensity with increasing temperature (Figure 10).

**3.3. Evolution of Solution Chemistry.** Insight into the evolution of the experiments described above can be gained by consideration of the saturation state of the fluid phase with respect to potential precipitating phases. The precipitation reactions for berlinite, variscite, and metavariscite are

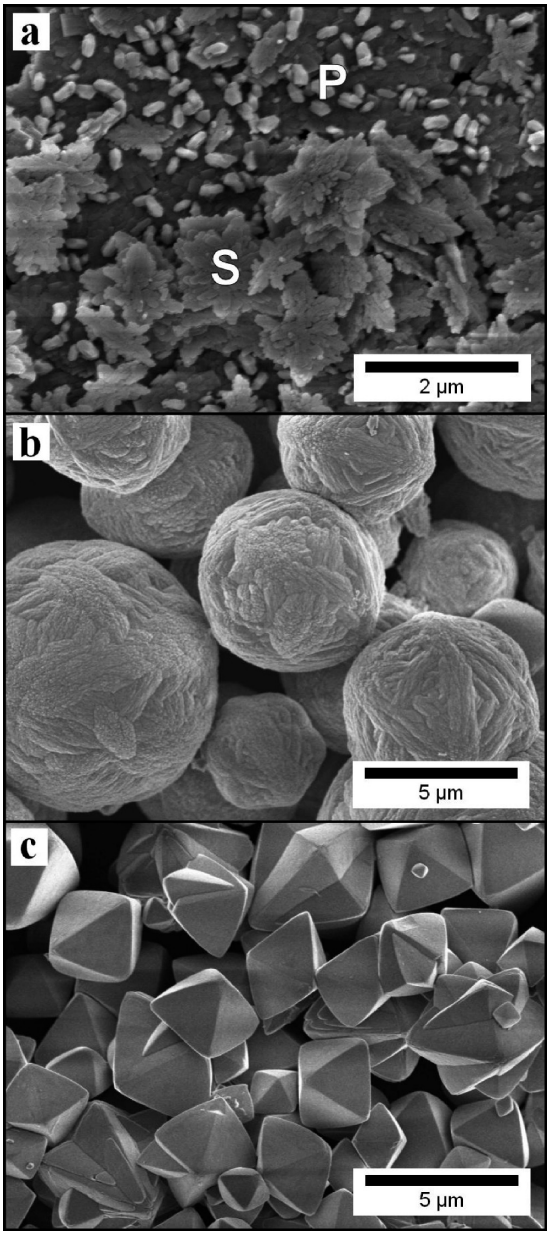


**Figure 8.** SEM photomicrographs of (a) mixed strengite (S) and phophosiderite (P) synthesized at $T$ = 100 °C for 9 days and of (b) ferric giniite synthesized at $T$ = 150 °C (c) and at $T$ = 200 °C for 12 h.

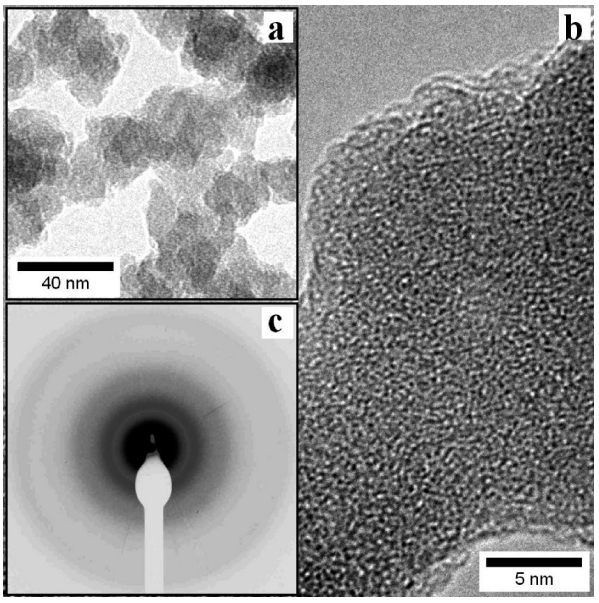


**Figure 9.** HR-TEM images of AFP: (a) general overview of particles; (b) high resolution detail from a single AFP grain; (c) electron diffraction pattern of grains shown in part b.

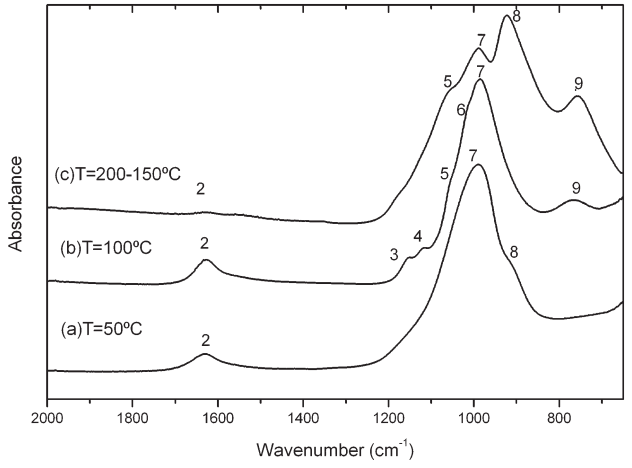


**Figure 10.** FTIR spectra of iron phosphate phases. Main bands are indicated by numbers above the spectra, and corresponding details of band assignements are described in Table 5 and in the text. Spectra: (a) AFP synthesized at temperature 50 °C at initial time; (b) mixed strengite and phosphosiderite synthesized at 100 °C after 9 days; (c) ferric giniite synthesized by heating at 150 or 200 °C for 12 h.

given by

$$Al^{3+} + PO_4^{3-} = \text{berlinite}$$

$$Al^{3+} + PO_4^{3-} + 2H_2O = \text{variscite}$$

and

$$Al^{3+} + PO_4^{3-} + 2H_2O = \text{metavariscite}$$

By adopting a standard state of unit activity for pure water, the ion activity products (IAP) of these three phases are identical and given by

$$IAP = a_{Al^{3+}} a_{PO_4^-}$$

Values of the IAP of berlinite, varsicite, and metavariscite in the initial and final fluids of each experiment are listed in Table 2. These IAP values decrease in all experiments, consistent with the precipitation of an aluminum phosphate phase. The saturation index of the final fluids in the 50 °C experiment is supersaturated with respect to both variscite and berlinite, consistent with the precipitation of the metastable amorphous phase (AAP). The saturation index of the final fluids in the 100 °C experiment is close to saturation with respect to variscite but supersaturated with respect to berlinite, consistent with variscite precipitation. At 150 and 200 °C, the final fluids are supersaturated with respect to berlinite but undersaturated with respect to variscite, consistent with berlinite precipitation. The S.I. for berlinite in these solutions suggests that the ion activity product is ~2 orders of magnitude higher than that for berlinite equilibrium. This suggests that the aqueous activities of $Al^{3+}$ and $PO_4^{3-}$ are on average approximately 1 order of magnitude greater in these solutions then they would be at equilibrium with berlinite. This difference can be due to several factors including the following: (1) the reactive solution has yet to attain equilibrium with the solid phase or (2) there are uncertainties in the thermodynamic database used to calculate the saturation index.

**Table 5. Main FTIR Bands for the Iron Phosphate Spectra in Figure 8**

| | wavenumber[a] ($cm^{-1}$) | | | | |
|---|---|---|---|---|---|
| band no. | (a) | (b) | (c) | bonds assignments[b] | ref |
| 1 | ~3496 | ~3597 | ~3348 | O−H $\nu$ | 62, 65 |
| 2 | ~1631 | ~1624 | ~1574 | H−O−H $\delta$ | 62, 65 |
| 3 | | ~1152 | | $PO_4$ $\nu$ | 62, 63, 65 |
| 4 | | ~1120 | | $PO_4$ $\nu$ | 62, 65 |
| 5 | | 1056 | ~1063 | $PO_4$ $\nu$ | 62, 63, 65 |
| 6 | | ~1013 | | $PO_4$ $\nu$ | 62, 63, 65 |
| 7 | ~985 | ~986 | ~989 | $PO_4$ $\nu$ | 62, 63, 65 |
| 8 | ~912 | | ~923 | $PO_4$ $\nu$ | 62, 65 |
| 9 | | ~767 | ~756 | Fe−O | 65 |

[a] (a) AFP synthesized at temperature 50 °C at initial time; (b) mixed strengite and phosphosiderite synthesized at 100 °C after 9 days; (c) ferric giniite synthesized by heating at 150 °C or 200 °C for 12 h. [b] $\nu$ = stretching; $\delta$ = bending.

For the iron phosphate system the precipitation reactions for ferric giniite, strengite, and phosphosiderite are given by

$$5Fe^{3+} + 4PO_4^{3-} + 3OH^- + 2H_2O = \text{ferric giniite}$$

$$Fe^{3+} + PO_4^{3-} + 2H_2O = \text{strengite}$$

and

$$Fe^{3+} + PO_4^{3-} + 2H_2O = \text{phosphosiderite}$$

and by again adopting a standard state of unit activity for pure water, the ion activity for strengite and phosphosiderite are given by

$$IAP = a_{Fe^{3+}} a_{PO_4^-}$$

and that for ferric giniite is given by

$$IAP = a^5_{Fe^{3+}} a^4_{PO_4^{3-}} a^3_{OH^-}$$

Values of the IAP of ferric giniite, strengite, and phosphosiderite of the initial and final fluids of each experiment are listed in Table 3. The IAP decreases in all the experiments, consistent with the precipitation of an iron phosphate phase. The saturation index of the final fluids in the 100 °C experiment is saturated with respect to strengite, consistent with its precipitation. The saturation index of the final fluids at

150 °C is close to saturation with respect to strengite, yet it is undersaturated with respect to strengite at 200 °C. The degree to which these solutions are saturated with respect to ferric giniite or other iron phosphate phases could not be assessed due to a lack of solubility data.

**3.4. Implications for Natural Fluids.** Thermodynamic calculations suggest that variscite and strengite are the least soluble phosphate bearing minerals in natural waters at temperature less than 50 °C and pH $< 7$.[3] The batch reactor experiments presented above show that amorphous Al and Fe phosphates rather than crystalline minerals precipitate initially from solutions supersaturated with respect to variscite and strengite at temperatures less than 100 °C. This observation suggests that amorphous phase precipitation rather than variscite or strengite precipitation limits the maximum phosphate concentration of acidic ambient temperature natural waters. In contrast, variscite dissolution experiments demonstrate that this mineral dissolves rapidly in undersaturated solutions.[66] If, as was seen in the 100 °C experiments, amorphous Al and Fe phosphate phases eventually transform into their crystalline counterparts, it might be reasonable to expect that variscite and strengite dissolution could provide a lower limit for phosphate availability in acidic ambient temperature natural waters. It therefore seems likely that water−solid reactions will fix phosphate concentrations to lie between the thermodynamic stability fields of crystalline variscite or strengite and their amorphous counterparts. In contrast, at $T = 100$ °C, amorphous Al and Fe phosphates transform within weeks to variscite and strengite. It is likely, therefore, that under such conditions these minerals may be able to buffer directly phosphate concentrations under acidic conditions. In either case, these results suggest that the addition of $Fe^{3+}$ could prove to be an effective means to lower dangerous phosphate concentrations if present in acidic natural waters.

## 4. Conclusion

The experiments presented above illustrate the systematic behavior of the solids formed from supersaturated solutions in the Al-$PO_4$−$H_2O$ and Fe−$PO_4$−$H_2O$ systems. At lower temperatures, amorphous phases (AAP and AFP) are initially favored and these can persist for substantial time. At elevated temperatures, crystalline berlinite and ferric giniite are formed rapidly, in the aluminum and iron system, respectively, via the amorphous precursors. The coexisting solutions in the aluminum system approach saturation with respect to variscite in less than 12 h at $T \leq 100$ °C and saturation with respect to berlinite at $T > 100$ °C. Similarly, the coexisting solutions in the iron-bearing experiments approach saturation with respect to strengite at 100 °C in experiments of 9 days duration. This observation of rapid solution equilibration suggests that the precipitation of phosphate minerals may be sufficiently fast to buffer phosphate concentrations in mildly acidic natural waters.

**Acknowledgment.** We thank Sam Shaw, Cristina Moisescu, Aryani Sumoondur (University of Leeds), and Elena Bazarkina (Université de Toulouse) for helpful discussions during the course of this study. Lesley Neve, Linda Forbes, Michael Ward and David Ashley (University of Leeds), and Alain Castillo (CNRS-Université de Toulouse) provided technical assistance. L.G.B. thanks A2 Technologies for their FTIR instrumentation support. Support from the Centre National de la Recherché Scientifique, University of Toulouse, the University of Leeds, and the European Community through the MIR Early Stage Training Network (MEST-CT-2005-021120) is gratefully acknowledged.

## References

(1) Oelkers, E. H.; Valsami-Jones, E. *Elements* **2008**, *4*, 83.
(2) Bennett, E. M.; Carpenter, S. R.; Caraco, N. F. *Bioscence*. **2001**, *51*, 227.
(3) Stumm, W.; Morgan J. J. *Aquatic Chemistry: An Introduction Emphasizing Chemical Equilibria in Natural Waters*; John Wiley and Sons: New York, 1981; p 780.
(4) Lindsay, W. L.; Moreno, E. C. *Soils Sci. Soc. Am. Proc*. **1960**, *24*, 177.
(5) Lindsay, W. L. *Chemical equilibria in soils*; John Wiley and Sons: New York, 1979.
(6) Moore, P. A. Jr.; Reddy, K. R.; Graetz, D. A. *Environ. Qual*. **1991**, *20*, 869.
(7) Huminicki, D. M. C.; Hawthorne, F. C. *Rev. Mineral. Geochem*. **2002**, *48*, 123.
(8) Kniep, R.; Mootz, D. *Acta Crystallogr*. **1973**, *B29*, 2292.
(9) Kniep, R.; Mootz, D.; Vegas, A. *Acta Crystallogr*. **1977**, *B33*, 263.
(10) Ng, H. N.; Calvo, C. *Can. J. Phys*. **1976**, *54*, 638.
(11) Fontanella, J. J.; Wintersgill, M. C.; Shannon, R. D.; Chai, B. H. T. *J. Phys. D: Appl. Phys*. **1993**, *26*, 101.
(12) Wagh, A. S.; Grover, S.; Jeong, J. *J. Am. Ceram. Soc*. **2003**, *86*, 1845.
(13) Drüppel, K.; Hösch, A.; Franz, G. *Am. Mineral*. **2007**, *92*, 1695.
(14) Moore, P. B. *Am. Mineral*. **1966**, *51*, 168.
(15) Song, Y.; Zavalij, P. Y.; Suzuki, M.; Whittingham, M. S. *Inorg. Chem*. **2002**, *41*, 5778.
(16) Nang, H. N.; Calvo, C. *Can. J. Chem*. **1975**, *53*, 2064.
(17) Reale, P.; Scrosati, B.; Delacourt, C.; Wurm, C.; Morcrette, M.; Masquelier, C. *Chem. Mater*. **2003**, *15*, 5051.
(18) Palache, C.; Berman, H.; Frondel, C. *Dana's system of mineralogy*; Volume II, Halides, nitrates, borates, carbonates, sulphates, arsenates, tungstates, molybdates. 7th ed.; Wiley: New York, and Chapman & Hall: London, Vol. II, 1951; p 1124.
(19) Ann, Y.; Reddy, K. R.; Delfino, J. J. *Ecol. Eng*. **2000**, *14*, 169.
(20) Dill, D. D. *Earth-Sci. Rev*. **2001**, *53*, 35.
(21) Dezzeo, N.; Chacón, N.; Sanoja, E.; Picón, G. *Forest Ecol. Manag*. **2004**, *200*, 183.
(22) Gammons, C. H.; Wood, S. A.; Pedrozo, F.; Varekamp, J. C.; Nelson, B. J.; Shope, C. L.; Baffico, G. *Chem. Geol*. **2005**, *22*, 249.
(23) Karathanasis, A. D. *Soil Sci. Soc. Am. J*. **1991**, *55*, 1774.
(24) Kumar, V.; Gilkes, R. J.; Bolland, M. D. A. *Fert. Res*. **1991**, *30*, 19.
(25) Nriagu, J. O.; Dell, C. L. *Am. Mieral*. **1974**, *59*, 934.
(26) Nriagu, J. O.; Moore, P. B. *Phosphate Minerals*; Springer-Verlag: Berlin, 1984; p 442.
(27) Kundeyarova, A. Y. *Geoderma* **1981**, *26*, 195.
(28) Bothe, J. V.; Brown, P. W. *J. Am. Ceram. Soc*. **1993**, *73*, 362.
(29) Exley, C.; Birchaill, J. D. *Polyhedron* **1992**, *11*, 1901.
(30) Gómez Morales, J.; Rodríguez Clemente, R.; Matijević, E. *J. Colloid Interface Sci*. **2004**, *151*, 555.
(31) Hsu, P. H. *Soil Sci*. **1982**, *133*, 305.
(32) Katsanis, E. P.; Matijević, E. *Colloids Surf*. **1982**, *5*, 43.
(33) Mata-Arjona, A.; Alario-Franco, M. A. *J. Therm. Anal*. **1973**, *5*, 319.
(34) McLaughlin, J. R.; Syers, J. K. *J. Soil Sci*. **1978**, *29*, 4994.
(35) Son, D.; Kim, E.; Kim, T.-G.; Kim, M. G.; Cho, J.; Park, B. *Appl. Phys. Lett*. **2004**, *85*, 5875.
(36) Van Riemsdijk, W. H.; Weststrate, F. A.; Bolt, G. H. *Nature* **1975**, *257*, 473.
(37) Warry, N. D.; Kramer, J. R. *Can. Mineral*. **1976**, *14*, 40.
(38) Anthony, J. W.; Bideaux, R. A.; Bladh, K. W.; Nichols, M. C. *Handbook of Mineralogy*; Volume 4, Arsenates, Phosphates, Vanadates; Mineral Data Publishing: Tucson, AZ, 2000; p 680.
(39) Onac, B. P.; White, W. B. *Am. Mineral*. **2003**, *88*, 1395.
(40) Linsday, W. L.; Vlek, P. L. G.; Chien, S. H. Phosphate Minerals. In *Minerals in soil environment*, 2nd ed.; Dixon, J. B., Weed, S. B., Eds.; SSSA Monograph; SSSA: Madison, WI, 1989; pp 1089−1130.
(41) Hesterbeg, D.; Zhou, W.; Hutchison, K. J.; Beauchemin, S.; Sayers, D. E. *J. Synchrotron Radiat*. **1999**, *6*, 636.
(42) D′Yvoire, F. B. *Soc. Chim. Fr*. **1961**, *7*, 2277.
(43) Delacourt, C.; Wurm, C.; Reale, P.; Morcrette, M.; Masquelier, C. *Solid State Ionics* **2004**, *173*, 113.

(44) Zaghib, K.; Julien, C. M. *J. Power Sources* **2005**, *142*, 279.
(45) Andersson, A. S.; Kalska, B.; Häggström, L.; Thomas, J. O. *Solid State Ionics* **2000**, *130*, 41.
(46) Okada, S.; Yamamoto, T.; Okazaki, Y.; Tokunaga, M.; Nishida, T. *J. Power Source* **2005**, *146*, 570.
(47) Dokko, K.; Koizumi, S.; Sharaishi, K.; Kanamura, K. *J. Power Sources* **2007**, *165*, 656.
(48) Yang, S.; Song, Y.; Ngala, K.; Zavalij, P. Y. *J. Power Sources* **2003**, *119*−*121*, 239.
(49) Rouzies, D.; Varloud, J.; Millet, J. M. M. M. *J. Chem. Soc., Faraday Trans.* **1994**, *90*, 3335.
(50) Bache, B. W. *Eur. J. Soil Sci.* **1964**, *15*, 110.
(51) Kuo, S. Phosphorus. In *Methods of soil analysis. Part 3*; Sparks, D. L., Ed.; Soils Science Society of America: Madison, WI, 1996.
(52) Violler, E.; Inglett, P. W. *Appl. Geochem.* **2000**, *15*, 785.
(53) PDF-2 Powder Diffraction File Database.
(54) Brunauer, S.; Emmett, P. H.; Teller, E. *J. Am. Chem. Soc.* **1938**, *60*, 309.
(55) Parkhurst, D. L.; Appelo, C. A. J. PHREEQC (Version 2)—A computer program for speciation, batch-reaction, one-dimensional transport and inverse geochemical calculations. *U.S. Geological Survey Water Resources Investigations Report* **1999**, 99.
(56) Johnson J.; Anderson G.; Parkhurst D. Database from "thermo.com.V8.R6.230" prepared at Lawrence Livermore National Laboratory (Revision: 1.11), 2000
(57) Ostwald, W. *Z. Phys. Chem., Stoechiom. Verwandtschaftsl.* **1900**, *34*, 495.
(58) Lundager Madsen, H. E. *J. Cryst. Growth* **2008**, *310*, 2602.
(59) Rodriguez-Blanco, J. D.; Shaw, S.; Benning, L. G. *Mineral. Mag.* **2008**, *72*, 283.
(60) Ogino, T. *Geochim. Cosmochim. Acta* **1987**, *51*, 2756.
(61) Pinzaru, S. C.; Onac, B. P. *Vib. Spectrosc.* **2009**, *49*, 97.
(62) Farmer, V. C. Mineralogical Society Monograph 4: The Infrared Spectra of Minerals. *Mineral. Soc.* **1974**.
(63) Frost, R. L.; Weier, M. L.; Erickson, K. L.; Carmody, O.; Mills, S. J. *J. Raman Spectrosc.* **2004**, *35*, 1047.
(64) Rokita, M.; Handke, M.; Mozagawa, W. *J. Mol. Struct.* **2000**, *555*, 351.
(65) Frost, R. L.; Wills, R.-A. *Spectrochim. Acta A* **2007**, *66*, 42.
(66) Roncal-Herrero, T.; Oelkers, E. H. *Mineral. Mag.* **2008**, *72*, 349.